Letters

Design and Implementation of Luenberger Model-Based Predictive Torque Control of Induction Machine for Robustness Improvement

Liming Yan and Xuding Song

***Abstract*—This letter proposes a Luenberger model-based predictive torque control (LM-PTC) of induction machine to compensate prediction error caused by mismatched parameters. In the traditional predictive torque control (T-PTC), stator current, stator flux vector, and electromagnetic torque are predicted in one sampling period by open-loop prediction model, which will inevitably lead to prediction error by mismatched parameters, first. Inspired by the idea of closed-loop Luenberger observer, in the torque and flux prediction, the feedback correction part is introduced into prediction equations for LM-PTC. Second, the steady prediction errors of T-PTC and LM-PTC are, respectively, analyzed with mismatched parameter. Finally, the proposed LM-PTC is verified by the comparison experiments including dynamic-state, transient-state, and steady-state experiments.**

***Index Terms*—Induction machine, mismatched parameter, model predictive control, robustment.**

I. Introduction

FOR power electronics and electric drive, finite control set-model predictive control (FCS-MPC) has been widely studied by scholars, because its exhaustive strategy is suitable for power electronic systems, and discrete control strategy is suitable for digital systems based on digital signal processor (DSP) [1], [2]. At present, there are two main problems in FCS-MPC, one is how to improve the prediction accuracy for mismatched prediction models, the other is how to design the cost functions and the weight coefficients. The first question will be discussed in this letter.

Scholars have made some research on the prediction accuracy of FCS-MPC. In [3], model predictive current control with mismatched parameters for three-phase inverter are analyzed, where current prediction error equation is established. In [4], for interior permanent magnet synchronous motor (IPMSM), the prediction errors of stator currents with mismatched stator resistance and mutual inductance are deduced. For the prediction errors caused by mismatched parameters, there are two main compensation methods for model prediction errors. One is model predictive control based on online parameter identification strategy, the other is model predictive control based on active disturbance rejection control (ADRC). The basic idea of the first method is to use online parameter identification technology to observe the parameters of induction motor or PMSM, and then refresh the parameters of the motor online, so as to improve the accuracy of the prediction model and the control performance of the system. In [5], model predictive power control of ac–dc active front ends with an adaptive online parameter identification technique is proposed to mitigate performance degradation caused by mismatched parameters. In [6], for the boost converter, online inductor parameters identification by a small-signal injection strategy is proposed to improve the accuracy of the prediction model. In [7], an incremental prediction model is proposed to eliminate the prediction error, where the inductance disturbance observer and inductance extraction strategy are presented based on sliding mode observer. In [8], model predictive current control of IPMSM with online least squares system identification is proposed to improve the control performance. The basic idea of the second method is to use ADRC theory to observe the prediction errors caused by mismatched parameters, and to compensate for the prediction errors by feedforward method. In [9], ADRC-based model predictive current control strategy is developed for PMSM, where ADRC is used to realize disturbance estimation and compensation. In [10], a disturbance observer-based model predictive torque control for induction motor is proposed to eliminate to load torque disturbances and parameter uncertainties. In [11], generalized proportional integral observer based model predictive current control for induction motor is presented to observe and eliminate time-varying disturbances. In [12], in FCS-PTC of induction machine, extended high-gain state observer is proposed to take the place of the proportional-integral controller, which further improves dynamic performance.

The above methods are mainly used to passively eliminate or reduce the prediction errors caused by mismatched parameters by combining other methods (online parameter identification or ADRC). In this letter, the prediction error is eliminated actively by modifying the prediction model itself. It is well known that in closed-loop flux observer, the correction compensation term is utilized to improve the accuracy of the observer. Similarly, in this letter, on the basis of open-loop predictive model of traditional predictive torque control (T-PTC), the correction compensation term is introduced to form Luenberger model-based predictive torque control, which is a closed-loop predictive model. In addition, the analysis theory of the steady prediction error is established in this letter by complex theoretical derivation. Section II introduces the mathematical model of induction machine. In Section III, the steady prediction error of T-PTC and LM-PTC with mismatched parameters are theoretically analyzed. Section IV makes the experimental research for T-PTC and LM-PTC, and Section V summarizes this letter.

II. Induction Machine Mathematical Model and T-PTC

In the stator reference frame, the mathematical model of induction machine is shown as (1)–(3), where $\boldsymbol{\psi_s} = L_s\boldsymbol{i_s} + L_m\boldsymbol{i_r}$ and $\boldsymbol{\psi_r} = L_r\boldsymbol{i_r} + L_m\boldsymbol{i_s}$. L_s, L_r, and L_m are stator inductance, rotor inductance,

Manuscript received July 3, 2019; revised August 24, 2019; accepted August 31, 2019. Date of publication September 2, 2019; date of current version December 13, 2019. *(Corresponding author: Liming Yan.)*

L. Yan is with the School of Automobile, Chang'an University, Xi'an 710064, China (e-mail: ylm@chd.edu.cn).

X. Song is with the Key Laboratory of Road Construction Technology and Equipment, Ministry of Education, Chang'an University, Xi'an 710064, China (e-mail: songxd@chd.edu.cn).

Color versions of one or more of the figures in this article are available online at http://ieeexplore.ieee.org.

Digital Object Identifier 10.1109/TPEL.2019.2939283

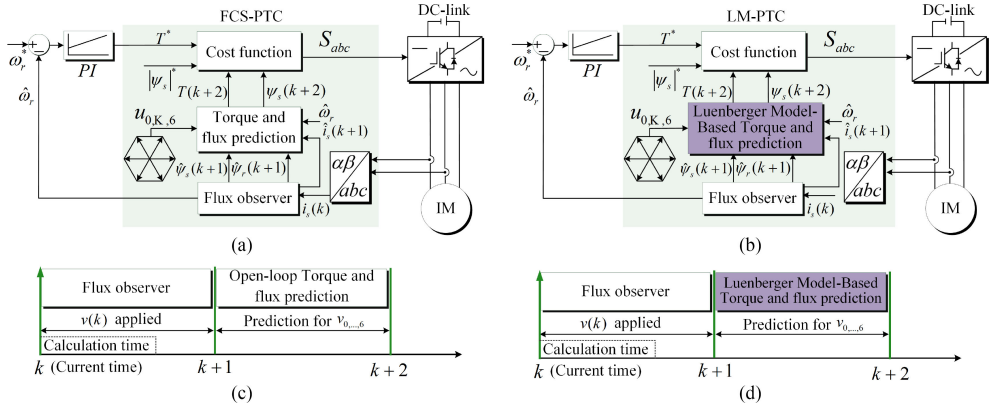

Fig. 1. (a) Block diagram of the T-PTC. (b) Execution of T-PTC in k sampling time. (c) Block diagram of the proposed LM-PTC. (d) Execution of the proposed LM-PTC in k sampling time.

and mutual inductance, respectively

$$\boldsymbol{v_s} = R_s \boldsymbol{i_s} + \frac{d}{dt}\boldsymbol{\psi_s} \tag{1}$$

$$0 = R_r \boldsymbol{i_r} + \frac{d}{dt}\boldsymbol{\psi_r} - j\omega_r \boldsymbol{\psi_r} \tag{2}$$

$$T_e = \frac{3}{2} p \mathrm{Im}\left\{\bar{\boldsymbol{\psi}}_{\boldsymbol{s}} \boldsymbol{i_s}\right\}. \tag{3}$$

Based on the above equations, the predictive equations of stator flux linkage and electromagnetic torque in T-PTC are expressed as (4)–(6). The equation (7) is the cost function, which is utilized to select the optimal voltage vector. Detailed implementation of T-PTC is elaborated in [11]

$$\psi_s(k+2) = \psi_s(k+1) + T_s v_s(k+1) - R_s T_s i_s(k+1) \tag{4}$$

$$i_s(k+2) = \left(1 - \frac{T_s}{\tau_\sigma}\right) i_s(k+1) + \frac{T_s}{\tau_\sigma}\frac{k_r}{R_\sigma} \cdot \left(\frac{1}{\tau_r} - jw\right) \cdot \psi_r(k+1) + \frac{T_s}{\tau_\sigma R_\sigma} v_s(k+1) \tag{5}$$

$$T_e(k+2) = \frac{3}{2} p \mathrm{Im}\left\{\bar{\psi}_s(k+2) \cdot i_s(k+2)\right\} \tag{6}$$

$$g = |T_e^* - T_e(k+2)| + \lambda_\psi \left||\psi_s|^* - |\psi_s(k+2)|\right| + I_{s\max}. \tag{7}$$

The block diagram and the execution of the conventional T-PTC are presented in Fig. 1(a) and (c), respectively. The T-PTC strategy mainly consists of three parts, flux observer, toque and flux prediction, and the cost function. In order to compensate for the time delay, the *estimation + prediction* approach is adopted and illustrated in Fig. 1(c).

III. Luenberger Model-Based Predictive Torque Control

The induction machine equations with stator current i_s and stator flux ψ_s as state variables are expressed in (8) and (9), where A_{11}, A_{21}, A_{12}, and B are shown in (10) and (11), respectively

$$\frac{di_s}{dt} = A_{11} i_s + A_{12} \psi_s + B u_s \tag{8}$$

$$\frac{d\psi_s}{dt} = A_{21} i_s + u_s \tag{9}$$

$$A_{11} = -\frac{1}{\sigma}\left(\frac{R_s}{L_s} + \frac{R_r}{L_r}\right) + j\omega_r, \quad A_{21} = -R_s \tag{10}$$

$$A_{12} = \frac{1}{\sigma}\left(\frac{R_r}{L_s L_r} - j\frac{\omega_r}{L_s}\right), \quad B = \frac{1}{\sigma L_s}, \quad \sigma = 1 - \frac{L_m^2}{L_s L_r}. \tag{11}$$

Therefore, stator flux observer of induction machine are expressed in (12) and (13). K_{12} ($K_{12} = k_1 + jk_2$) and K_{34} ($K_{34} = k_3 + jk_4$) are the parameters of observer

$$\hat{i}_s(k+1) = \hat{i}_s(k) + T_s\left[A_{11}\hat{i}_s(k) + A_{12}\hat{\psi}_s(k) + B u_s(k)\right] + T_s K_{12}\left(\hat{i}_s(k) - i_s(k)\right) \tag{12}$$

$$\hat{\psi}_s(k+1) = \hat{\psi}_s(k) + T_s\left[A_{21}\hat{i}_s(k) + u_s(k)\right] + T_s K_{34}\left(\hat{i}_s(k) - i_s(k)\right). \tag{13}$$

In T-PTC, the predictive equations of stator current $i_s(k+2)$ and stator flux $\psi_s(k+2)$ is shown in (4) and (5), and the concrete implementation of T-PTC is shown in Fig. 1(a) and (c), where open-loop torque and flux equations are applied. In this letter, Luenberger model-based torque and flux predictions are proposed to compensate for the prediction errors caused by mismatched parameters, which are shown in (14) and (15). Because $i_s(k+1)$ cannot be measured in the sampling time k, $i_s(k+1)$ can be estimated by Lagrange extrapolation equation,

$$i_s(k+1) = \sum_{l=0}^{n} (-1)^{n-l} \begin{bmatrix} n+1 \\ l \end{bmatrix} i_s(k+l-n)$$

$$\hat{i}_s(k+2) = T_s\left[A_{11}\hat{i}_s(k+1) + A_{12}\hat{\psi}_s(k+1) + B u_s(k+1)\right] + T_s K_{12}\left(\hat{i}_s(k+1) - i_s(k+1)\right) + \hat{i}_s(k+1) \tag{14}$$

$$\hat{\psi}_s(k+2) = \hat{\psi}_s(k+1) + T_s\left[A_{21}\hat{i}_s(k+1) + u_s(k+1)\right] + T_s K_{34}\left(\hat{i}_s(k+1) - i_s(k+1)\right). \tag{15}$$

The block diagram and the execution of the proposed LM-PTC are presented in Fig. 1(b) and (d), respectively. The proposed LM-PTC strategy mainly contains three parts, flux observer, Luenberger model-based toque and flux prediction, and the cost function. Similarly, the *estimation + prediction* approach is adopted to compensate for time

delay, which is illustrated in Fig. 1(d). The part of Luenberger model-based torque and flux prediction is proposed to eliminate the prediction errors caused by mismatched parameters.

The parameter sensitivity analysis of Luenberger model-based torque and flux prediction is to obtain an analytical relation between the predicted flux and the actual flux, by taking the mismatched parameters into account. This relation can be obtained in the steady states. Owing to $di_s/dt = j\omega i_s$, $d\psi_s/dt = j\omega\psi_s$ in the steady state of induction machine, the actual flux of induction machine satisfies the following:

$$j\omega i_s = A_{11} i_s + A_{12}\psi_s + Bu_s \tag{16}$$

$$j\omega\psi_s = A_{21} i_s + u_s. \tag{17}$$

Similarly, in steady state, the predicted flux satisfies the following (18) and (19), where the continuous Luenberger model-based torque and flux predictions are adopted for convenient analysis. A_{11}^*, A_{12}^*, A_{21}^*, and B^* represent the mismatched parameters. For example, $A_{21}^* = -R_s^*$, and R_s^* is the corresponding mismatched parameter of R_s

$$j\omega\hat{i}_s = A_{11}^*\hat{i}_s + A_{12}^*\hat{\psi}_s + B^*u_s + K_{12}(\hat{i}_s - i_s) \tag{18}$$

$$j\omega\hat{\psi}_s = A_{21}^*\hat{i}_s + u_s + K_{34}(\hat{i}_s - i_s). \tag{19}$$

By combining (16)–(19) and eliminating $\hat{i}$, i_s, and u_s, the relation of the predicted flux $\hat{\psi}_s$ and the actual flux ψ_s is expressed in (20), where A_0, B_0, C_0, G, and H are presented as

$$A_0\hat{\psi}_s + (B_0G + C_0H)\psi_s = 0 \tag{20}$$

$$A_0 = \frac{A_{11}^* + K_{12} - j\omega}{A_{21}^* + K_{34}}\cdot j\omega + A_{12}^*,$$

$$C_0 = -\frac{A_{11}^* + K_{12} - j\omega}{A_{21}^* + K_{34}} + B^* \tag{21}$$

$$B_0 = \frac{A_{11}^* + K_{12} - j\omega}{A_{21}^* + K_{34}}\cdot K_{34} - K_{12},\ G = \frac{A_{12} + j\omega B}{BA_{21} - A_{11} + j\omega} \tag{22}$$

$$H = \left[\frac{j\omega(j\omega - A_{11})}{A_{21}} - A_{12}\right] \Big/ \left(B + \frac{j\omega - A_{11}}{A_{21}}\right). \tag{23}$$

Therefore, the predicted flux error $|\hat{\psi}_s/\psi_s|$ and the predicted flux angle error ρ_e are expressed in (24) and (27), where $A_{01} = \mathrm{Re}(A_0)$, $A_{02} = \mathrm{Im}(A_0)$, $B_{01} = \mathrm{Re}(B_0)$, $B_{02} = \mathrm{Im}(B_0)$, $C_{01} = \mathrm{Re}(C_0)$, $C_{02} = \mathrm{Im}(C_0)$, $G_1 = \mathrm{Re}(G)$, $G_2 = \mathrm{Im}(G)$, $H_1 = \mathrm{Re}(H)$, $H_2 = \mathrm{Im}(H)$.

$$\left|\frac{\hat{\psi}_s}{\psi_s}\right| = \sqrt{q_1^2 + q_2^2},\ \ \rho_e = \text{angle}\left(\hat{\psi}_s, \psi_s\right) = \text{arctg}\left(-q_2/q_1\right) \tag{24}$$

$$q_1 = \frac{-A_{01}Z_1 - A_{02}Z_2}{A_{01}^2 + A_{02}^2},\ \ q_2 = \frac{A_{02}Z_1 - A_{01}Z_2}{A_{01}^2 + A_{02}^2} \tag{25}$$

$$Z_1 = B_{01}G_1 - B_{02}G_2 + C_{01}H_1 - C_{02}H_2 \tag{26}$$

$$Z_2 = B_{02}G_1 + B_{01}G_2 + C_{02}H_1 + C_{01}H_2. \tag{27}$$

Similarly, by combining (16)–(19) and eliminating $\hat{\psi}_s$, ψ_s, and u_s, the predicted current error $|\hat{i}_s/i_s|$ and the predicted current angle error $\rho_e^{'}$ can be deduced in (28)–(33), where $A_{01}^{'} = \mathrm{Re}(A_0^{'})$, $A_{02}^{'} = \mathrm{Im}(A_0^{'})$, $B_{01}^{'} = \mathrm{Re}(B_0^{'})$, $B_{02}^{'} = \mathrm{Im}(B_0^{'})$, $C_{01}^{'} = \mathrm{Re}(C_0^{'})$, $C_{02}^{'} = \mathrm{Im}(C_0^{'})$, $H_1^{'} = \mathrm{Re}(H^{'})$, $H_2^{'} = \mathrm{Im}(H^{'})$

$$\left|\frac{\hat{i}_s}{i_s}\right| = \sqrt{\left(q_1^{'}\right)^2 + \left(q_2^{'}\right)^2},\ \ \rho_e^{'} = \text{arctg}\left(-q_2^{'}/q_1^{'}\right) \tag{28}$$

$$q_1^{'} = \frac{-A_{01}^{'}Z_1^{'} - A_{02}^{'}Z_2^{'}}{\left(A_{01}^{'}\right)^2 + \left(A_{02}^{'}\right)^2},\ \ q_2^{'} = \frac{A_{02}^{'}Z_1^{'} - A_{01}^{'}Z_2^{'}}{\left(A_{01}^{'}\right)^2 + \left(A_{02}^{'}\right)^2} \tag{29}$$

$$Z_1^{'} = B_{01}^{'} + C_{01}^{'}H_1^{'} - C_{02}^{'}H_2^{'} \tag{30}$$

$$Z_2^{'} = B_{02}^{'} + C_{02}^{'}H_1^{'} + C_{01}^{'}H_2^{'} \tag{31}$$

$$A_0^{'} = \frac{A_{12}^*\left(A_{21}^* + K_{32}\right)}{j\omega},\ \ B_0^{'} = A_{11}^* - j\omega - \frac{A_{12}^*K_{34}}{j\omega} \tag{32}$$

$$C_0^{'} = \frac{A_{12}^*}{j\omega} + B^*,\ \ H^{'} = \left(j\omega - A_{11} - \frac{A_{12}A_{21}}{j\omega}\right) \Big/ \left(\frac{A_{12}}{j\omega} + B\right). \tag{33}$$

From (24)–(27) and the (10)–(11), it can be seen that the parameters of the computational formulas of the predicted flux error $|\hat{\psi}_s/\psi_s|$ and the predicted flux angle error ρ_e are L_s, L_m, L_r, R_s, R_r, L_s^*, L_m^*, L_r^*, R_s^*, R_r^*, ω, ω_r. In order to analyze $|\hat{\psi}_s/\psi_s|$ and ρ_e under different torques T_e and speeds ω_m conditions, ω_r and ω should be computed according to T_e and ω_m, first. The computing equations of ω_r and ω are presented in (34) and (35) [13]. Second, compute $|\hat{\psi}_s/\psi_s|$ and ρ_e based on (24)–(27). Third, Fig. 2 is made according to the predicted flux errors and predicted flux angle errors calculated under different torques and speeds. The plotting process is shown in Fig. 3. In particular, in the analytical expressions of the predicted flux error $|\hat{\psi}_s/\psi_s|$ and the predicted flux angle error ρ_e, when $K_{12} = 0$ and $K_{34} = 0$, those are the prediction errors of open-loop torque and flux prediction for T-PTC. The above calculation process is also applicable to the calculation of $|\hat{i}_s/i_s|$ and $\rho_e^{'}$

$$\omega_{sr} = \frac{4}{3p}\frac{T_e}{|\psi_{\text{sref}}|^2}\frac{R_rL_s^2}{L_m^2} \tag{34}$$

$$\omega_r = p\omega_m,\ \ \omega = \omega_r + \omega_{sr}. \tag{35}$$

Theoretical results of the prediction errors of T-PTC and LM-PTC with $R_s^* = 2.0R_s$ and $L_m^* = 0.5L_m$ are presented in Fig. 2. It can be seen that the flux prediction errors $|\hat{\psi}_s/\psi_s|$ and the flux angle prediction errors ρ_e of the proposed LM-PTC are smaller than those of the conventional T-PTC when $R_s^* = 2.0R_s$. When $L_m^* = 0.5L_m$, it has the same rules. In addition, the prediction errors $|\hat{\psi}_s/\psi_s|$ and ρ_e has a very low sensitivity to the stator resistance, and a high sensitivity to the mutual inductance.

IV. Experimental Comparison of T-PTC and LM-PTC

In this section, the comparative experiments are made to verify the proposed LM-PTC on the experimental test of 2.2-kW induction machine, which is shown in Fig. 4. The parameters of induction machine are as follows: $R_s = 2.68\ \Omega$, $R_r = 2.13\ \Omega$, $L_m = 0.275$ H, $L_s = 0.283$ H, $L_r = 0.283$ H, $\omega_{\text{nom}} = 2772$ r/min, $|\psi_s|^* = 0.71$ Wb. The experimental results are shown in Fig. 5. Fig. 5(a) and (b) are the general performances of T-PTC and LM-PTC, respectively, where the speed command varies from 2772 to -2772 r/min at 0.3 s. Fig. 5(c) and (d) are the transient performances of T-PTC and LM-PTC, respectively, where the load torque suddenly is exerted at 4.0 s. The response time of the electromagnetic torque for LM-PTC are only 760 μs, which is 10.59% faster than that of T-PTC. Fig. 5(e) and (f) are the steady-state

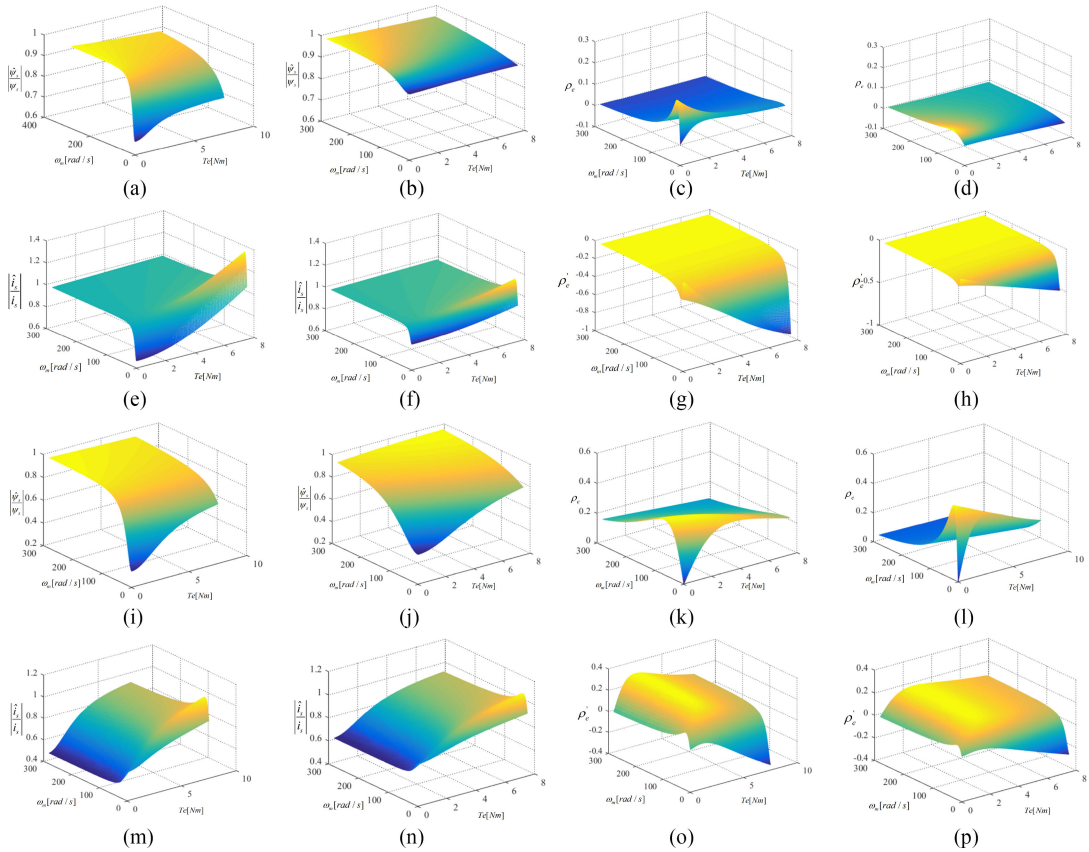

Fig. 2. (a) and (b) are flux prediction errors with $R_s^* = 2.0R_s$ for T-PTC and LM-PTC, respectively. (c) and (d) are flux angle prediction errors with $R_s^* = 2.0R_s$ for T-PTC and LM-PTC, respectively. (e) and (f) are current prediction errors with $R_s^* = 2.0R_s$ for T-PTC and LM-PTC, respectively. (g) and (h) are current angle prediction errors with $R_s^* = 2.0R_s$ for T-PTC and LM-PTC, respectively. (i) and (j) are flux prediction errors with $L_m^* = 0.5L_m$ for T-PTC and LM-PTC, respectively. (k) and (l) are flux angle prediction errors with $L_m^* = 0.5L_m$ for T-PTC and LM-PTC, respectively. (m) and (n) are current prediction errors with $L_m^* = 0.5L_m$ for T-PTC and LM-PTC, respectively. (o) and (p) are current angle prediction errors with $L_m^* = 0.5L_m$ for T-PTC and LM-PTC, respectively.

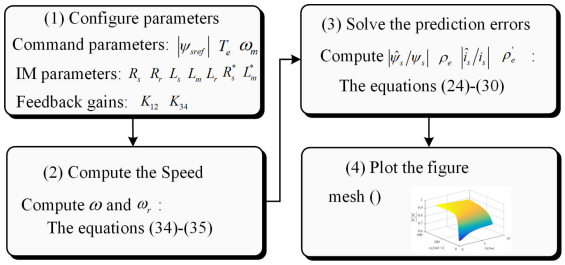

Fig. 3. Plotting process of the prediction errors for LM-PTC and T-PTC.

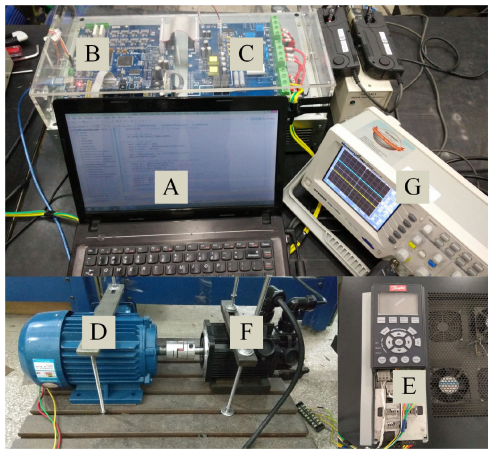

Fig. 4. Experimental platform. (A) Computer. (B) DSP. (C) Power drive module. (D) Induction machine. (E) PMSM. (F) Danfoss inverter. (G) Oscilloscope.

performances of T-PTC and LM-PTC, where the total harmonic distortion (THD) of stator current of LM-PTC is 9.52% and that of T-PTC is 12.16%. In Fig. 5(f), it is seen that the electromagnetic torque ripple of T-PTC is 1.5 Nm. The electromagnetic torque ripple of LM-PTC is 1.0 Nm, which is 33.3% smaller than that of T-PTC. This is because in each control cycle, the feedback correction mechanism improves the prediction accuracy of the electromagnetic torque, and then reduces the electromagnetic torque ripple.

The experimental results of LM-PTC and T-PTC with mismatched parameters are illustrated in Fig. 6, where the speed command is 1500 r/min and the load torque is 3.5 N·m. R_s and L_m are the measured parameters of induction machine, and R_s^* and L_m^* are the mismatched parameters that are used in the LM-PTC controller and T-PTC controller. From Fig. 6(a) and (b), it can be seen that stator current THD of LM-PTC with $R_s^* = 2.0R_s$ is 9.83%, which is 27.56% lower than that of T-PTC with $R_s^* = 2.0R_s$. From Fig. 6(a) and (c), it can be seen that LM-PTC has a lower sensitivity to R_s, compared

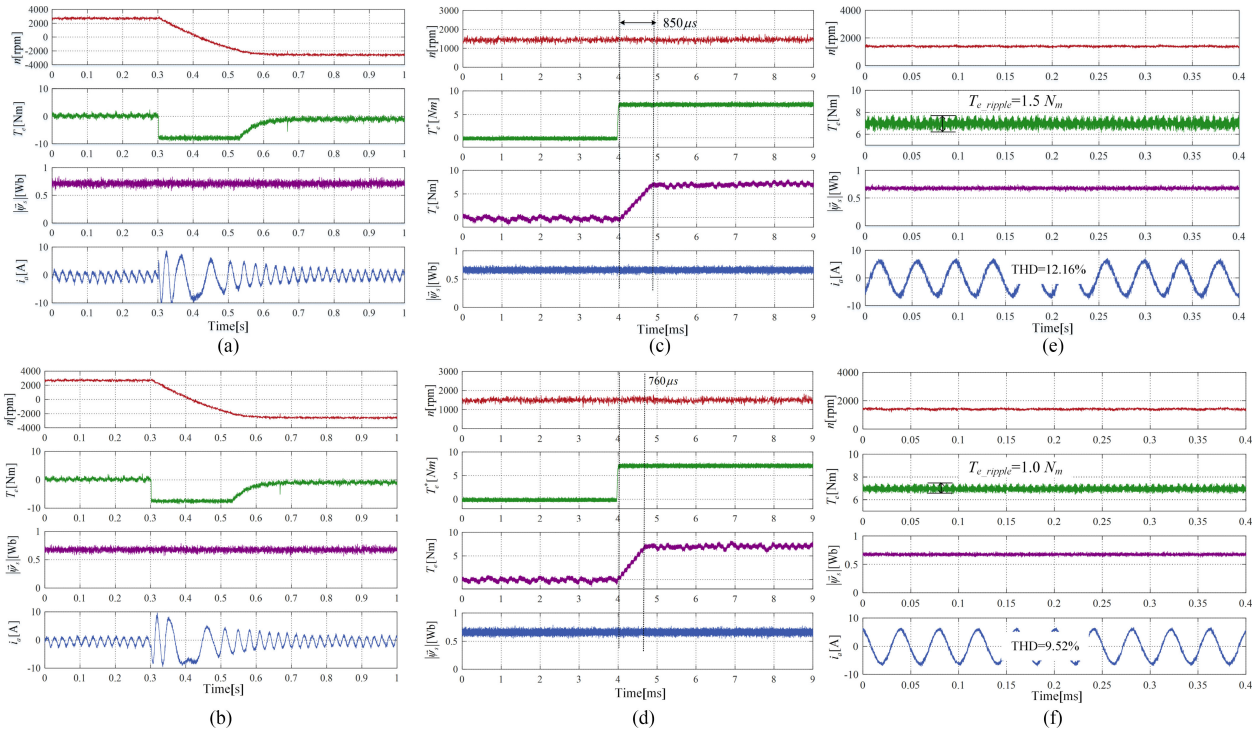

Fig. 5. Experimental comparison of T-PTC and LM-PTC. (a) General performance of T-PTC. (b) General performance of LM-PTC. (c) Transient performance of T-PTC. (d) Transient performance of LM-PTC. (e) Steady performance of T-PTC. (f) Steady performance of LM-PTC.

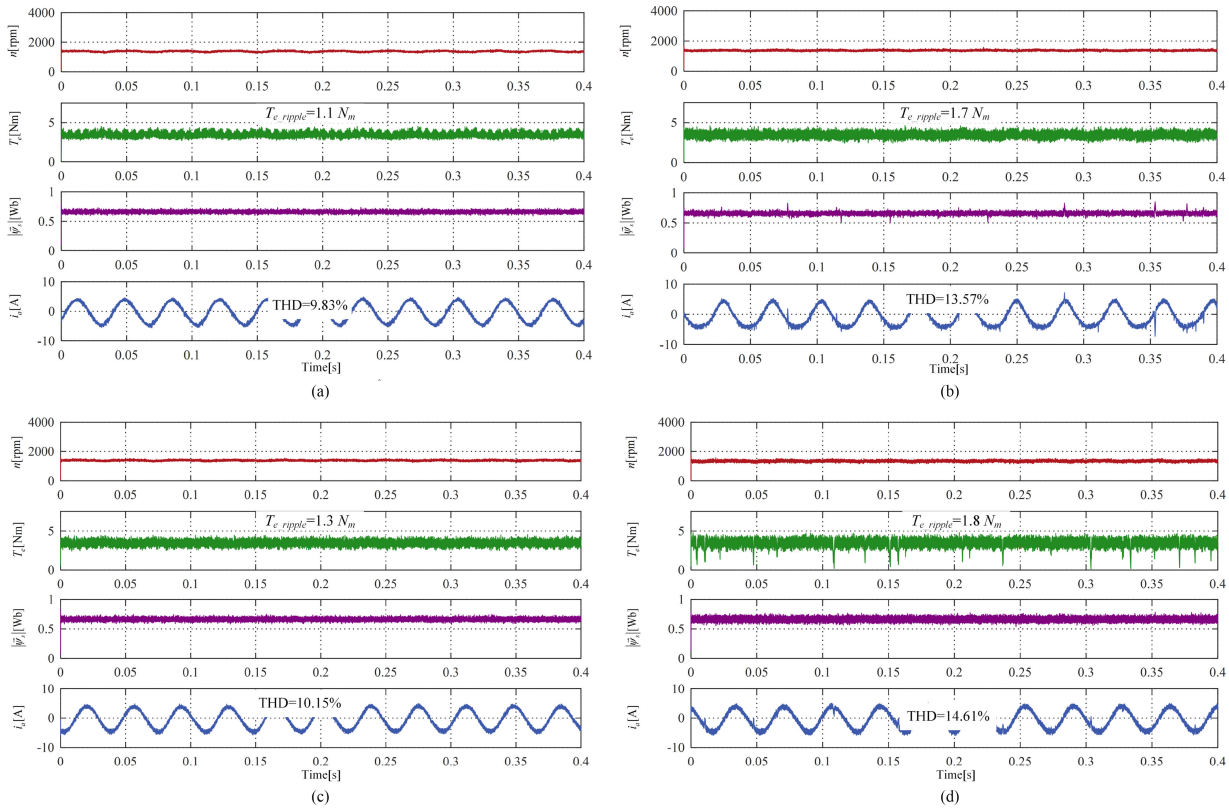

Fig. 6. Experimental results of the proposed LM-PTC and traditional T-PTC with mismatched parameters. (a) LM-PTC with $R_s^* = 2.0R_s$. (b) T-PTC with $R_s^* = 2.0R_s$. (c) LM-PTC with $L_m^* = 0.5L_m$. (d) T-PTC with $L_m^* = 0.5L_m$.

with L_m. The experimental results are consistent with the theoretical analysis in Section III.

V. Conclusion

It is known that FCS-PTC depends on the parameters, which leads the torque and flux prediction error and then reduces the control performance. Except for active disturbance rejection technology and online parameter identification to compensate for the prediction error, this letter proposes Luenberger model-based predictive torque control, where the closed-loop torque and flux prediction equations can eliminate the prediction errors. The analytical expressions of prediction errors with mismatched parameters are first presented in this letter. Finally, the experimental results verify the effectiveness of the proposed LM-PTC.

References

[1] S. Vazquez, J. Rodríguez, M. Rivera, L. G. Franquelo, and M. Norambuena, "Model predictive control for power converters and drives: Advances and trends," *IEEE Trans. Ind. Electron.*, vol. 64, no. 2, pp. 935–947, Feb. 2017.

[2] P. Cortes, M. P. Kazmierkowski, R. M. Kennel, D. E. Quevedo, and J. Rodríguez, "Predictive control in power electronics and drives," *IEEE Trans. Ind. Electron.*, vol. 55, no. 12, pp. 4312–4324, Dec. 2008.

[3] H. A. Young, M. A. Perez, and J. Rodríguez, "Analysis of finite-control-set model predictive current control with model parameter mismatch in a three-phase inverter," *IEEE Trans. Ind. Electron.*, vol. 63, no. 5, pp. 3100–3107, May 2016.

[4] M. Siami, D. A. Khaburi, and J. Rodríguez, "Torque ripple reduction of predictive torque control for PMSM drives with parameter mismatch," *IEEE Trans. Power Electron.*, vol. 32, no. 9, pp. 7160–7168, Sep. 2017.

[5] S. Kwak, U. Moon, and J. Park, "Predictive-control-based direct power control with an adaptive parameter identification technique for improved AFE performance," *IEEE Trans. Power Electron.*, vol. 29, no. 11, pp. 6178–6187, Nov. 2014.

[6] C. Chen *et al.*, "Online inductor parameters identification by small-signal injection for sensorless predictive current controlled boost converter," *IEEE Trans. Ind. Inform.*, vol. 13, no. 4, pp. 1554–1564, Aug. 2017.

[7] X. Zhang, L. Zhang, and Y. Zhang, "Model predictive current control for PMSM drives with parameter robustness improvement," *IEEE Trans. Power Electron.*, vol. 34, no. 2, pp. 1645–1657, Feb. 2019.

[8] S. Hanke, S. Peitz, O. Wallscheid, J. Bocker, and M. Dellnitz, "Finite-control-set model predictive control for a permanent magnet synchronous motor application with online least squares system identification," in *Proc. IEEE Int. Symp. Predictive Control Elect. Drives Power Electron.*, May 2019, pp. 1–6.

[9] Q. Teng, G.-F. Li, J. Zhu, Y. Guo, and S. Li, "ADRC-based model predictive current control for PMSMs fed by three-phase four-switch inverters," in *Proc. IEEE 8th Int. Power Electron. Motion Control Conf.*, May 2016, pp. 2724–2731.

[10] J. Wang, F. Wang, Z. Zhang, S. Li, and J. Rodrłguez, "Design and implementation of disturbance compensation-based enhanced robust finite control set predictive torque control for induction motor systems," *IEEE Trans. Ind. Inform.*, vol. 13, no. 5, pp. 2645–2656, Oct. 2017.

[11] J. Wang, F. Wang, G. Wang, S. Li, and L. Yu, "Generalized proportional integral observer based robust finite control set predictive current control for induction motor systems with time-varying disturbances," *IEEE Trans. Ind. Inform.*, vol. 14, no. 9, pp. 4159–4168, Sep. 2018.

[12] F. Wang, J. Wang, R. M. Kennel, and J. Rodrłguez, "Fast speed control of ac machines without the proportional-integral controller: Using an extended high-gain state observer," *IEEE Trans. Power Electron.*, vol. 34, no. 9, pp. 9006–9015, Sep. 2019.

[13] Y. Wang, T. Ito, and R. D. Lorenz, "Loss manipulation capabilities of deadbeat direct torque and flux control induction machine drives," *IEEE Trans. Ind. Appl.*, vol. 51, no. 6, pp. 4554–4566, Nov. 2015.